Volume 1 | Number 1 | Jan 2013 | Pages 1–100

Dalton Transactions

An international journal of inorganic chemistry
www.rsc.org/dalton

ROYAL SOCIETY OF CHEMISTRY

ROYAL SOCIETY OF CHEMISTRY

www.rsc.org/dalton

Dalton Transactions

ARTICLE

Behaviour of Surface Hydroxide Groups of Exfoliated Kaolinite in Gas Phase and during Water Adsorption

Attila Táborosi [a] and Róbert K. Szilágyi [b,*]

The chemical and physical properties, thus the reactivity of phylloaluminosilicates can be tailored by intercalation, delamination, and exfoliation processes. In going from the periodic crystalline to the molecular exfoliated phase, surface defects and modifications gain importance as each face of the phylloaluminosilicate becomes in direct contact with the external chemical environment. In this work, we extend our earlier studies on molecular cluster modelling of exfoliated kaolinite sheets by evaluating the positions and orientations of surface hydroxide groups and bridging oxide anions, as sites of reactivity. The previous focus on inner chemical environment of a single kaolinite layer is shifted to the surface exposed octahedral aluminium-hydroxide and tetrahedral silicon-oxide sheets. Combination of semi-empirical, *ab initio* wave function, and density functional calculations unanimously support the amphoteric nature of the surface hydroxide groups with respect to H-bonding donor/acceptor capabilities. To a lesser extent, we observe the same for the bridging oxide anions. This is in contrast with the crystalline phase, which manifests only donor orientation for maintaining inter-layer H-bond network. These results suggest that both electrophilic and nucleophilic characteristics of the octahedral and tetrahedral sheets need to be considered during intercalation and concomitant exfoliation of the kaolinite sheets.

Introduction

Kaolinite is the simplest phylloaluminosilicates with 1:1 ratio of aluminium octahedral (O) and silicon tetrahedral (T) sheets forming an OT-layer. Kaolinite is a non-swelling clay in water; however, with a limited set of small organic molecules (urea, ethylene glycol, hexylamine) and salts (ammonium or potassium acetate) it can form organoclay hybrid materials via intercalation.[1-5] The mechanisms of intercalation, exchange intercalation, and exfoliation with elimination of crystallinity are not yet understood at the molecular level. However, this is desirable for rationalized design of hybrid nanoclay materials. We approached these mechanistic questions from the exfoliated state (Fig. 1B) given that it can be probed by a very limited set of analytical techniques than the crystalline phase (Fig. 1A). We have already laid the foundation for utilizing molecular cluster models based on coordination chemistry principles.[6-8] The surface hydroxide (s-HO$^-$), inner hydroxide (i-HO$^-$), apical oxide (a-O^{2-}), and bridging oxide (b-O^{2-}) groups were treated as ligands to the Al^{3+} and Si^{4+} centres (Fig. 1). The smallest coordination units for a single octahedral and tetrahedral site are $[Al^{3+}(\mu^2$-s-HO$^-)_3(\mu^2$-i-HO$^-)(\mu^3$-a-O$^{2-})_2]^{4-}$ and $[Si^{4+}(\mu^3$-a-O$^{2-})(\mu^2$-b-O$^{2-})_3]^{4-}$, respectively. Additional Al^{3+} and Si^{4+}

ions from the outer sphere along with their ligands surround these inner coordination sphere environments. We consider a honeycomb-like unit as the building block of the molecular model due to its importance in adsorption of small molecules, and thus in intercalation and exfoliation processes.
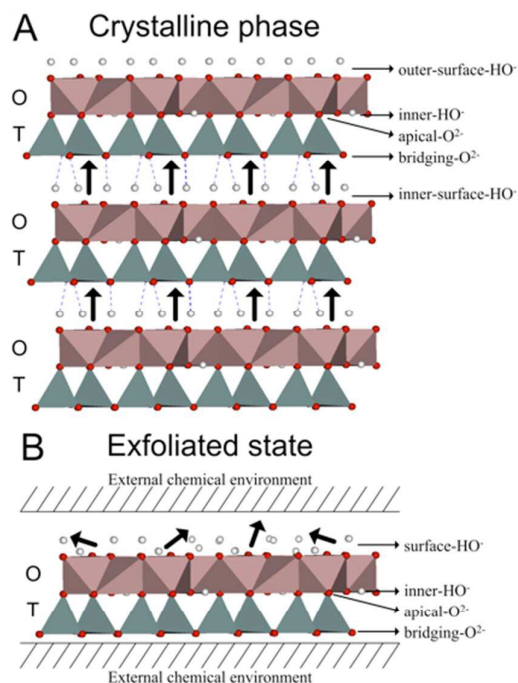
Fig. 1 Structural and compositional features of crystalline (A) and exfoliated (B) kaolinite (pink: octahedral Al^{3+} centres; grey: tetrahedral Si^{4+} centres).

[a.] Department of Environmental Engineering, Faculty of Engineering, University of Pannonia, Veszprém, H-8201, PO Box 10, Hungary.

[b.] Department of Chemistry and Biochemistry, Montana State University, Bozeman, MT 59717, U.S.A. and MTA-ELTE Chemical Structure&Function "Momentum" Research Lab, Budapest, 1117, Hungary

* Correspondence: szilagyi@montana.edu or szilagyirk@chem.elte.hu.
Electronic Supplementary Information (ESI): Cartesian coordinates; formatted checkpoint files from computational.chemistry.montana.edu/clay4

The position and orientation of the surface hydroxide groups of an exfoliated kaolinite sheet (Fig. 1B) are quintessential in determining acid/base properties of the surface, thus its reactivity. For example, rotation of the s-HO$^-$ groups along the Al$\cdots$Al axes can create nucleophilic sites and induce Lewis base behaviour. The s-HO$^-$ groups are electrophilic when they are perpendicular to the O-sheet as in the crystalline phase. Simultaneous presence of perpendicular and parallel s-HO$^-$ groups with respect to the O-sheet can result in an amphoteric pattern of Lewis acid/base characteristics.

The role of s-HO$^-$ groups in clay reactivity has been shown in numerous computational studies. A key difference to previous works,[9, 10] is that we consider all possible orientations in a systematic grid-like mapping. Therefore, we provide a complete potential energy landscape description with both global and local minima in comparison to those sampled by molecular dynamics (MD) or Monte Carlo (MC) methods. In addition, we carried out an extensive evaluation of structural dependence of the level of theory. Based on our previous works,[6-8] the overly truncated computational models[11] manifest numerous artificial H-bonding interactions and arbitrary constraints need to be applied. Thus, they cannot provide a chemically reasonable picture for the s-HO$^-$ orientation. The seminal work by Tunega et $al.$[12] using periodic models and plane wave-based LDA and GGA level of theory already indicated the flexibility of the surface hydroxide groups even in the crystalline phase. They discussed a competition between the inter-layer and intra-layer H-bonding. In the periodic crystalline unit, the energy difference between the folded and perpendicular s-HO$^-$ was found to be 14 kJ mol^{-1}. In agreement with our previous findings,[7] as the surface hydroxide groups distort from their crystalline positions, the inner hydroxide groups also move in sync. For a hypothetical isolated kaolinite and a dickite layer[13] using two-dimensional periodic models, MD simulations revealed that at room temperature and in gas phase, fluctuation of various surface hydroxide groups can take place. Two structures were discussed with s-HO$^-$ groups adjacent and on top of the i-HO$^-$ groups that manifested the most movement. The former can adopt positions between the perpendicular as in the crystal structure and parallel positions in a folded conformation, while the other s-HO$^-$ groups remained unchanged relative to the crystalline phase.

Similarly to the s-HO$^-$ positions, wettability or water coverage of kaolinite surface was studied by various periodic boundary models. Man-Chao and Jian[10] investigated the adsorption and migration of water on kaolinite with LDA functionals and plane wave basis set. They found that at low coverage, the H$_2$O molecule preferentially absorbs at the three-fold hollow sites with a binding energy of approximately 100 kJ mol^{-1}. Two of the s-HO$^-$ groups form H-bonds with the adsorbed H$_2$O molecule, while the adsorbate also H-bonds to a folded down s-HO$^-$ group. At high water coverage[9] using molecular mechanical force field[14] and various water models, a 'nanodroplet' of water (500–1,000 molecules) was found to spread out at the O-sheet and form a monolayer. The same

simulations showed that for the T-sheet, the water 'nanodroplet' stays together as a deformed sphere with a contact angle of about 105°. The experimental value for contact angle of approximately 20° indicates that the kaolinite surface is overall hydrophilic.[15] An extensive DFT study with GGA functionals and plane wave pseudo-potentials[16] corroborated previous results showing that the preferred structure of water accepts two H-bonds from and donates one H-bond to the O-sheet. Clustering of water molecules was not found to be significant as they dissociated from the O-surface. Unexpectedly, ice-like growth was not observed with multiple layers of water molecules due a "hydrophobic behaviour of the layered water". They proposed that the amphoteric characteristic of the O-sheet might be a key to wettability of kaolinite.

The aim of the present systematic investigation was to extend our previous study of inner coordination environment of an OT-layer to the outer surfaces of the O- and T-sheets. We created two separate molecular cluster models that describe both the inner and outer spheres of the [6Al-6(s-HO$^-$)] (Al-honeycomb) and [6Si-6(b-O^{2-})] (Si-honeycomb) moieties, respectively. These conceptually converged, coordination chemistry-based molecular cluster models allowed for interpretations of FTIR spectroscopic features for the inner hydroxide stretching modes as indicators for the external chemical environments.[17]

It is important to highlight that in contrast to the inner hydroxide group, the surface hydroxide groups and bridging oxide anions have an ill-defined coordination environment (Fig. 1). Within an OT-layer, the inner-hydroxide immediate coordination environment remains practically as in crystalline phase. However, upon exfoliation, the properties of the surface hydroxide groups and bridging oxide anions will be greatly determined by the external chemical environment. Therefore, we considered both ends of the chemical environment spectrum from gas phase to aqueous solution phase with explicit solvation and dielectric continuum. The former is a realistic model for a clean surface before dehydroxylation above 350 °C.[18] The aqueous phase model has explicit solvation of a ring of six H$_2$O molecules with H-bonding interactions to the surface hydroxide groups and the bridging oxide anions in the O- and T-sheet models, respectively.

Methodology

Computational Models

All computational models were derived from a combined X-ray and inelastic neutron diffraction experimental crystal structure of kaolinite[19, 20] obtained from the FIZ Karlsruhe Inorganic Structural Database[21, 22] (structure reference number 078401). The construction steps of the molecular cluster model were defined in details in the previous publication.[7] The inner sphere coordination environments for the crystalline O-sheet, exfoliated O-sheet, and exfoliated T-sheet honeycomb units are shown in Figs. 2A, 2B, and 2C, respectively. The initial structures of the computational models with the neutralizing
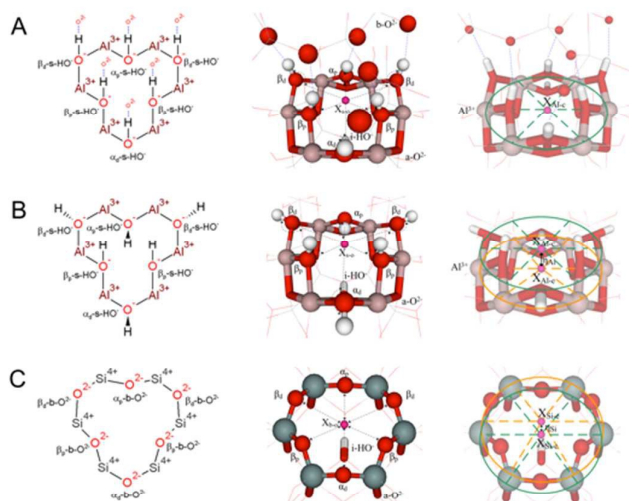
Fig. 2 The orientations of the surface hydroxide groups and bridging oxide anions, Al^{3+} and Si^{4+} ion positions in crystalline (A) and exfoliated kaolinite models (B) for the Al-honeycomb and (C) for the Si-honeycomb.

counter ions are shown in Fig. 3. In addition to the previously described centres and groups (Fig. 1), we defined additional structural elements as the centroids of the various honeycomb units. X_{s-HO}, X_{b-O}, X_{Al}, and X_{Si} represent the centroid of six oxygen atoms in s-OH$^-$ and b-O^{2-}, the centroid of six Al^{3+} and Si^{4+} ions, respectively. The η_{Al} and η_{Si} values in Å correspond to the displacement of the crystalline (experimental) and exfoliated (calculated) planes of Al^{3+} and Si^{4+} ions, respectively. The sizes of the honeycomb-like units were characterized by their diameters (d_{Al} and d_{Si} in Å), which were derived from a diameter for a circle from the circumference of the honeycombs. The s-HO$^-$ groups had to be differentiated as three of them (proximal) located closer to the centre of the honeycomb (X_{s-HO}) than the other three (distal), which are the proximal groups of adjacent honeycombs. There is an additional classification of the surface hydroxide groups that we adopted, which is their relative position to the inner hydroxide group. The α_p-s-HO$^-$ and α_d-s-HO$^-$ groups are the proximal and distal surface hydroxide groups above the i-HO$^-$ groups as shown in Figs. 2A and 2B. The pairs of β_p-s-HO$^-$ and β_d-s-HO$^-$ groups are located above the a-O^{2-} groups (Figs. 2A and 2B). The complexity of labelling is required, since the positions of HO$^-$ groups and O^{2-} anions matter a great deal as will be shown below.

A change in the orientation of the s-HO$^-$ group relative to the surface can be followed by the centroid X_{s-HO}⋯O-H(s-HO$^-$) angles. In the crystalline kaolinite, these values are around 90° as the s-HO$^-$ groups in the inter-layer space point toward the T-sheet of an adjacent OT-layer. Similarly for the T-sheet, the α-b-O^{2-} and β-b-O^{2-} anions are located under the i-HO$^-$ groups and between the a-O^{2-} groups, respectively as shown in Fig. 2C. Change in the positions of the b-O^{2-} anions can be represented by the centroid X_{b-O}⋯O(b-O$^-$) distances. Only partial geometry optimizations were carried out for the inner sphere environment of the surface hydroxide groups and the
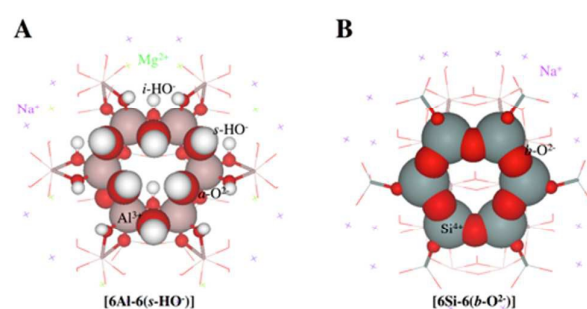
Fig. 3 Molecular cluster models for the (A) Al-honeycomb and (B) Si-honeycomb (space filling CPK), inner (ball and stick) and outer spheres (tubes), neutralizing ions (violet and light green crosses) with compositions of $[Al_{12}(s\text{-HO}^-)_{24}(i\text{-HO}^-)_{16}(a\text{-O}^{2-})_{16}Si_8(b\text{-O}^{2-})_{16}Na_{12}Mg_8]^0$ and $[Si_{12}(b\text{-O}^{2-})_{24}(a\text{-O}^{2-})_{12}Al_{10}(i\text{-HO}^-)_7(s\text{-HO}^-)_{17}Na_{18}]^0$, respectively.

adjacent Al^{3+} ions, as well as the bridging oxide and their Si^{4+} neighbouring ions (Fig. 3, atoms presented with ball-and-stick style) while the outer sphere ions and groups, and the counter-ions were kept frozen at their crystal structure positions (Fig. 3, atoms presented with bonds-only style).

We also considered periodic models in addition to the molecular cluster models for the exfoliated state in order to evaluate the performance of the levels of theory and use a comprehensive coverage of computational models. The periodic boundary model (PBC[23-25]) for the crystalline phase contained a single unit cell (1×1×1 supercell), while the exfoliated state was approximated by a four unit cell slab model (2×2 supercell) along the crystallographic 'a' and 'b' directions.

Computational Levels of Theories

For comparability of the inner and surface hydroxide cluster models, we used the same set of basis sets and set of density functionals as rationalized by Scheme 2 of Ref. 7. The molecular structure simulations were carried out using the Gaussian09[26] suite of quantum chemical packages. The computational level of theory included pure DFT functionals with Becke's exchange and Lee-Yang-Parr's correlation (BLYP)[27-29] and Perdew-Wang's exchange and correlation (PW91) functionals,[30, 31] Becke's empirically adjusted hybrid exchange and Lee-Yang-Par's correlation functionals (B3LYP),[28, 32] and pure molecular orbital (MO) calculations at the Hartree-Fock (HF) level.[33] Abbreviation HFLYP stands for a hybrid DFT method where the complete density functional exchange term was replaced by HF exchange, while keeping the full Lee-Yang-Parr correlation functional. We have studied the basis set effect by considering effective core potentials (ECP: SDD[34, 35]) and all electron basis sets (DZ: 6-31G[36, 37] and TZ: def2-TZVP[38, 39]) with polarization[40-42] (ECP* or DZ*) and diffuse[43] functions (DZ+, DZ+*). An isotropic electrostatic environmental effect on the exfoliated clay models was considered by using a polarizable continuum model (PCM[44] and COSMO[45]) with water-based parameters. For an approximate treatment of dispersion interactions, we utilized the empirical dispersion correction developed by Grimme.[46]

ARTICLE   **Dalton Transactions**

Table 1 Comparison of unit cell parameters (a, b (c) in Å and α (β, γ) in degrees for crystalline and slab models) as a function of level of theory relative to experimental values.

Level of theory	a	b	c	α	β	γ
crystalline phase						
Experimental[19,20]	5.15	8.94	7.16	91.7	104.6	89.8
periodic crystalline model: 1×1×1						
PW91/ECP	0.18	0.34	0.22	-0.6	0.5	-0.4
PW91/DZ*	0.08	0.13	0.27	0.1	0.3	0.0
BP86/DZ*	0.09	0.15	0.28	0.1	0.3	-0.1
PW91/TZ*	0.06	0.11	0.34	0.0	0.0	0.0
BP86/TZ*	0.07	0.13	0.33	-0.1	0.0	0.0
exfoliated state without an experimental reference						
periodic slab model: 2×2						
PW91/ECP	0.19	0.38				-2.1
PW91/TZ*	0.03	0.08				-1.7
BP86/TZ*	0.03	0.10				-1.6

Results and Discussion

Experimental Structure *versus* Periodic Unit Cell Models

The motivation of comparing the arrangements of s-HO⁻ groups in the experimental and calculated crystalline structures is to define the accuracy of basis sets and selected density functionals. The calculated unit cell parameters relative to their experimental values are summarized in Table 1, as a global measure for structural agreement.

As found earlier,[7] the double-ζ quality basis sets (ECP) without polarization functions do not provide reasonable unit cell parameters with vector lengths being 0.2-0.3 Å. Additional polarization basis functions greatly improve the 'a' and 'b' unit cell dimensions; however, the inter-layer H-bonding is calculated to be weak compared to experiment that results in expansion of the unit cell along the (001) direction. In going from double- (DZ) to triple-ζ (TZ) quality basis set, there are some improvements along the dimensions of the OT-sheets; however, the agreement actually worsens in the inter-layer distance. This suggests that the pure DFT or GGA density functional methods used are not adequate to describe the H-bonding interactions. As discussed in literature,[47, 48] the use of hybrid functionals and dispersion corrections may improve the agreement between experiment and theory.

The internal coordinates in the crystalline phase provide further details about the accuracy of calculations. The s-HO⁻ groups need to maintain their orientation for H-bonding with the bridging oxide anions of the adjacent OT-sheet. The experimental structural parameters in Table 2 clearly show the different orientation of the proximal (67 and 73°) and distal (107 and 115°) s-HO⁻ groups for a honeycomb-like unit and also the difference between the s-HO⁻ groups above (α, 67 and 115°) the i-HO⁻ and in between (β, 73 and 107°) the a-O²⁻ groups. Both pure GGA functionals (BP86 and PW91) closely reproduce the crystal structure already at the DZ basis set level as long as polarization functions are present. This was not the case for the i-HO⁻, which delicate position was only maintained when TZ quality basis set was used. We justify the performance of the DZ* basis set with the fact that s-HO⁻ is

Table 2 Summary of s-HO⁻ orientation expressed by centroid $X_{s\text{-}HO⁻}$...O-H(s-HO⁻) angles in degrees as function of levels of theory in crystalline phase and exfoliated state of kaolinite; η_{Al} is the measure of out-of-plane displacements in Å of Al^{3+} ions, and Δd_{Al} is the relative diameter of the Al-honeycomb (d_{Al}(experimental) = 5.69 Å).

Level of theory	α_p-s-HO⁻	β_p-s-HO⁻		α_d-s-HO⁻	β_d-s-HO⁻		η_Al	Δd_Al, Å
crystalline phase								
experimental[19,20]	66.5	72.7	72.5	114.9	106.8	106.7		0.00
periodic 1×1×1 crystalline model								
PW91/ECP	67.2	67.2	65.2	113.8	114.1	112.6		0.20
PW91/DZ*	66.0	72.5	72.2	115.5	107.1	106.6		0.08
BP86/DZ*	66.0	72.5	72.1	115.6	107.1	106.6		0.09
PW91/TZ*	66.1	72.0	71.9	115.3	107.5	107.1		0.07
BP86/TZ*	65.5	71.0	71.3	115.4	107.9	108.3		0.08
exfoliated state without an experimental reference								
periodic 2×2 slab model								
PW91/ECP	23.3	62.1	55.5	155.6	123.9	117.7		0.23
PW91/TZ*	1.4	88.5	104.6	176.8	87.0	71.0		0.03
BP86/TZ*	2.0	100.7	97.1	176.0	78.6	74.1		0.05
molecular cluster model for the Al-honeycomb (Fig. 3A)								
HF/ECP	35.0	60.6	61.2	170.9	150.9	150.3	-0.09	0.02
HF/DZ	32.9	61.8	62.5	172.3	152.0	151.4	-0.09	0.02
HF/DZ*	7.8	72.9	77.3	177.8	172.7	172.7	-0.09	0.01
HF/TZ	31.3	63.6	64.4	173.2	152.4	152.0	-0.09	0.02
HF/TZ*	13.8	71.7	73.9	177.5	167.6	167.4	-0.10	0.01
HFLYP/TZ*	2.0	68.1	70.2	176.9	166.0	165.7	-0.12	0.02
B3LYP/ECP	20.4	65.5	66.4	175.4	160.4	160.1	-0.08	0.01
B3LYP/DZ	20.0	66.0	66.9	175.6	159.5	159.4	-0.07	0.01
B3LYP/DZ+D	11.6	66.3	66.9	177.4	163.6	163.4	-0.08	0.01
B3LYP/DZ+PCM	11.5	70.7	71.9	170.1	161.7	160.0	-0.05	0.04
B3LYP/DZ*	4.9	75.1	81.4	175.7	176.5	175.4	-0.08	-0.01
B3LYP/TZ	15.8	69.7	70.9	177.4	162.3	162.3	-0.08	0.01
B3LYP/TZ*	10.0	75.3	78.1	179.9	171.4	171.3	-0.08	0.00
BLYP/TZ*	10.3	75.4	78.2	179.7	171.6	171.4	-0.07	-0.02
BP86/TZ*	5.6	76.3	79.6	177.7	174.9	174.9	-0.07	0.00
PW91/TZ*	6.7	76.7	80.0	178.1	174.2	174.2	-0.08	0.00

involved in a stronger and more directional inter-layer ion/dipole interactions than the intra-layer interactions of i-HO⁻. Thus, a lower quality, less flexible basis set (DZ*) may also reproduce the crystal structure. A holistic measure of the Al-honeycomb geometry is its diameter (d_{Al} in Å). The experimental value for d_{Al} is about 5.7 Å. This is approximated within 0.1 Å for any of the periodic crystalline models with sufficiently large basis set. As the size of the basis set increases or we vary the nature of the functionals, the agreement improves for periodic models, but not significantly.

Looking at the differences in unit cell parameters and internal coordinates of the periodic 1×1×1 crystalline models we can suggests the likely due to error cancellations from using small basis set and GGA density functionals with out dispersion correction and HF exchange the non-saturated calculations with DZ* basis set can give reasonable structures.

Periodic 1×1×1 Crystalline *versus* 2×2 Slab Models

A reasonable agreement in the unit cell parameters in Table 1 between the 2D periodic lattice structures and the 3D experimental crystal structure is fortuitous. The slab model does not have any inter-layer interaction, thus it should be considered as a compositionally identical, but structurally very different chemical system. However, we wish to use the slab calculations as a reference for the molecular cluster based models. Starting the optimization from the crystal structure,

the periodic 2×2 models show a different degree of systematic changes in the orientation of the *s*-HO⁻ groups. An asymmetry, also called misfit or slip between the O- and T-sheets, exists due to the presence of the *i*-HO⁻. As we found earlier,[7] the different chemical environment of *i*-HO⁻ relative to the *a*-O²⁻ ions at the centre of an OT-layer manifests in the polarization of the *b*-O²⁻ anions at the T-sheet and in the orientation of the *s*-HO⁻ groups of the O-sheet, as shown in Table 2. In the exfoliated structure, the α-*s*-HO⁻ groups fold in and become parallel with the plane of the OT-sheet. The proximal α-*s*-HO⁻ group points toward (~0°) the centroid X_{s-OH}, while the distal points away from it (~180°). The β-*s*-HO⁻ groups remain in H-bonding donor position with respect to external chemical environment. The interaction between the folded in α-*s*-HO⁻ groups and the perpendicular β-*s*-HO⁻ groups can be described by a non-ideal H-bonding with a strong ion/dipole component. The H(α_p-*s*-HO⁻)···O(β_p-*s*-HO⁻) distances are 2.58±0.01 Å at B3LYP/TZ* level showing great variability with the size of the basis set (2.60±0.01 Å at B3LYP/DZ).

It is also interesting to note that the periodic slab models, especially at the PW91/TZ* level, approach the experimental unit cell dimensions better than the periodic crystalline models; however any improvement in the 'a' and 'b' dimensions is at the expense of the angle between the two unit cell vectors. Similarly the diameter of the Al-honeycomb (d_{Al}) is calculated within 0.03 Å of the experiment, which is again better than the crystal calculations.

Periodic 2×2 Slab *versus* Molecular Cluster Models for Exfoliated Kaolinite

The bottom part of Table 2 compares the results of systematic evaluation of the performance of computational methods.[7] It is remarkable that regardless of the level of theory the exfoliated state can be characterized by folded α-*s*-HO⁻ groups with angles 2-30°, while the β-*s*-HO⁻ groups remain perpendicular to the OT-sheet in the molecular cluster model. A notable difference in the molecular cluster model relative to the periodic slab model is the different orientation of the β_d-*s*-HO⁻ groups that show their nucleophilic face to the external chemical environment with X_{s-HO}···O-H(*s*-HO⁻) angles of 180°. This difference is understandable since the coordination chemical environment of the distal *s*-HO⁻ groups is incomplete due to the lack of adjacent Al-honeycombs. Furthermore, without exception the movement of the Al³⁺ ions toward the centre of the OT-layer was observed (η_{Al} values between -0.05 and -0.10 Å) similarly to the earlier study due to lack of external H-bonding interactions. This makes the proton of the *s*-HO⁻ groups more acidic, which reduces the covalent nature of the Al³⁺–O(*s*-HO⁻) bonds. In turn the Al³⁺–*a*-O²⁻ bonds gain more covalency manifesting shorter bonds and sinking of the Al³⁺ ions into the OT-layer. Despite these sizeable changes, the approximate diameter (d_{Al}) of the Al-honeycomb remains similar to that in the crystalline phase within 0.02 Å.

The trends observed for the *s*-HO⁻ group orientations are somewhat different from those described for the *i*-HO⁻ groups

as a function of the levels of theory. Using small basis sets, the changes are modest in the exfoliated model relative to the crystal structure. The use of finer integration grid does not influence the geometry significantly; however, dispersion correction and the presence of a polarizable continuum show an enhanced ion/dipole interaction between the folded α- and β-*s*-HO⁻ groups. This will be further highlighted in this study when explicit solvent interactions will be considered. The importance of the presence of additional polarization basis function can be seen comparing the results of DZ and DZ* and separately TZ and TZ* regardless of the level of theory. The α_p-*s*-HO⁻ group folds in more and in turn, the β_p-*s*-HO⁻ groups become more erected. Using the saturated TZ* basis set, the orientation of the α_p-*s*-HO⁻ group range from 2° (HFLYP), 6–7° (BP86, PW91), and 10° (BLYP and B3LYP) to 13° (HF). We conclude that the inherent nature of the exchange and correlation functionals will determine the strength of the ion/dipole interactions that drives the rearrangements of the surface hydroxide groups.

From the results of *in vacuo* calculations of the Al-honeycomb model, we can establish reference values for the orientation of the surface hydroxide groups. X_{s-HO}···O-H(*s*-OH⁻) angles between 60°–120° correspond to vertical arrows in Figs. 1A and 1B with a typical values of 70° for proximal and 110° for distal *s*-HO⁻ groups that are ±20° from the perpendicular (90°) orientation. This orientation is referred to electrophilic (E) arrangement with respect to ion/dipole or donor (D) orientation in H-bonding interactions. When the X_{s-HO}···O-H(*s*-OH⁻) angle is between 0°–60° (for proximal) and 120°–180° (for distal), the surface hydroxide adopts a nucleophilic (N) or acceptor (A) orientation in H-bonding. This scenario is represented by the close to horizontal arrows in Fig. 1B.

Surface Hydroxide Orientations for the Honeycomb Cluster Models in the Absence of An External Chemical Environment

In order to localize all local and global stationary structures, we carried out a systematic, grid-like search for the geometry and relative energies of different structures corresponding to the perpendicular and parallel orientation of the proximal *s*-HO⁻ groups with the most complete coordination environment.

Without any external chemical environment, we can establish a well-defined reference for the surface hydroxide orientations. This state of the exfoliated clay particle is relevant for cleaned and thermally treated samples below the dehydroxylation temperatures (at 350 °C and above) after removal of adsorbed small molecules. The three proximal *s*-HO⁻ groups were considered in both nucleophilic/H-bond acceptor (nucleophilic: N or acceptor: A) and electrophilic/H-bond donor (electrophilic: E or donor: D) arrangements giving rise to eight isomers. In the single shot, *in vacuo* modelling (Table 2) starting from the crystal structure, we only obtained a single orientation with α_p-*s*-HO⁻ becoming parallel (N or A) with the surface and the other two β_p-*s*-HO⁻ groups remain perpendicular (E or D).
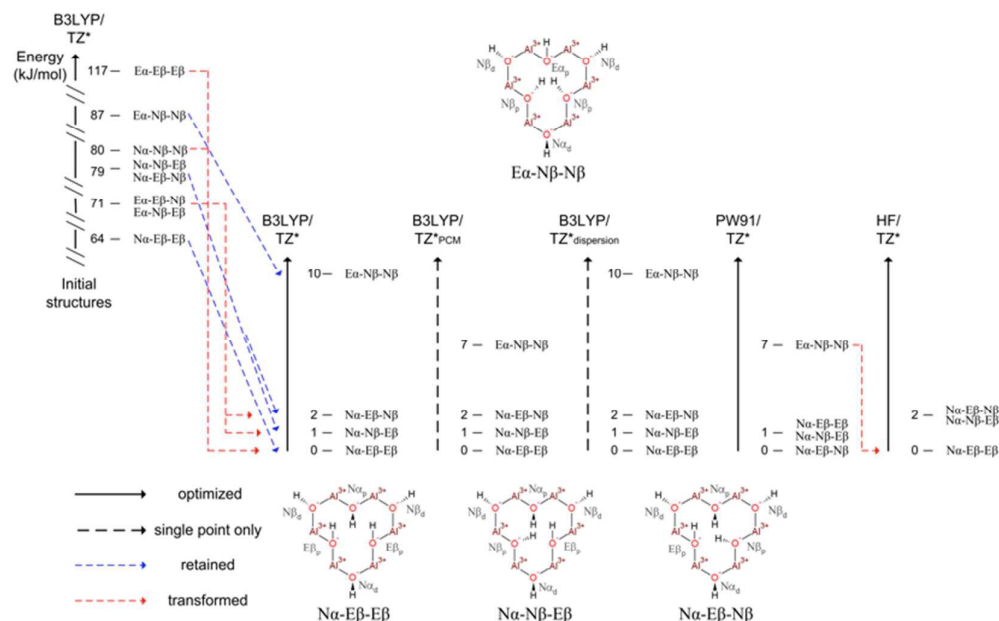
Fig. 4 Results of structural optimizations at various levels of theory for the orientations of the three proximal s-HO$^-$ groups located toward the centre of the Al-honeycomb for the *in vacuo* model of exfoliated kaolinite from HF, GGA, and hybrid-DFT calculations with TZ* basis set. Initial structures were obtained from the crystalline phase atomic positional coordinates with adjustments according to electrophilic (E) or nucleophilic (N) orientations. Arrows indicate isomerization as a result of going from one level of theory to the other upon structural optimizations.

Fig. 4 summarizes the relative energies of the orientations and how they interconvert shown by dashed lines as a function of level of theory. To avoid artefacts due to basis set effects, we report the results of saturated TZ* basis set. The initial structures were obtained by setting the centroid $X_{s\text{-HO}}\cdots$O-H(s-HO$^-$) angles to the ideal values of 10° (folded) and 70° (perpendicular) for the s-HO$^-$ groups. The orientations of the distal s-HO$^-$ groups were left as in the crystalline structure. The high initial energy is due to the erected positions of the distal s-HO$^-$ groups that fold down during structural relaxations.

Upon optimization, the proximal s-HO$^-$ groups relax within a 10 kJ mol^{-1} range and four species emerge as shown at the bottom of Fig. 4. In the periodic and earlier molecular cluster calculations, the s-HO$^-$ groups above the i-HO$^-$ fold in and become parallel with the surface for the three lowest energy structures (Nα-Eβ-Eβ). In gas phase simulations, one of the adjacent s-HO$^-$ groups can also fold in and adopt a low-energy orientation resulting in two folded s-HO$^-$ (Nα-Nβ-Eβ or Nα-Eβ-Nβ arrangements) groups, while the third remains erected. In all calculations, the reverse arrangement to the most stable orientation (Eα-Nβ-Nβ, top of Fig. 4) is at a highest energy (7-10 kJ mol^{-1}). It is also notable that while HF theory gives practically identical results for the i-HO$^-$ group to DFT,[7] the results for the s-HO$^-$ groups differ at HF and DFT levels. The use of polarizable continuum model (PCM) for simulating the electrostatic effect of a high dielectric (water) solvent environment or considering dispersion correction affect the relative ordering of orientations only as much as the variation of the results as a function of functional (B3LYP *versus* PW91, see Fig. 4).

Table 3 Summary of s-HO$^-$ group orientations as defined by the centroid $X_{s\text{-HO}}\cdots$O-H(s-HO$^-$) angle (degrees) as function of levels of theory in the exfoliated molecular cluster model.

Orientation	Level of theory	α_p-s-HO$^-$	β_p-s-HO$^-$		α_d-s-HO$^-$	β_d-s-HO$^-$	
Nα-Eβ-Eβ	HF/TZ*	13.8	71.7	73.9	177.5	167.6	167.4
	B3LYP/TZ*	10.0	75.3	78.1	179.9	171.4	171.3
	PW91/TZ*	6.7	76.7	79.9	178.1	174.2	174.2
Nα-Nβ-Eβ	HF/TZ*	26.4	32.6	90.4	176.2	164.5	166.1
	B3LYP/TZ*	24.3	28.0	94.4	178.9	169.5	170.6
	PW91/TZ*	22.7	26.7	96.1	178.8	171.8	173.2
Nα-Eβ-Nβ	HF/TZ*	27.7	88.8	30.1	175.9	166.1	163.8
	B3LYP/TZ*	25.5	93.9	26.8	178.8	170.5	168.4
	PW91/TZ*	24.4	94.8	25.8	178.8	172.8	170.8
Eα-Nβ-Nβ	HF/TZ*	spontaneous conversion to Nα-Eβ-Eβ					
	B3LYP/TZ*	82.2	27.1	29.4	178.5	169.7	169.4
	PW91/TZ*	90.8	20.3	25.6	179.1	172.7	172.6

The numerical results for the orientation of the s-HO$^-$ groups summarized in Table 3 clearly illustrate the co-planar (small angle values or close to 180°) and perpendicular (angle values around 90°) arrangements relative to the exfoliate kaolinite surface. The s-HO$^-$ groups that fold in correspond to a centroid $X_{s\text{-HO}}\cdots$O-H(s-HO$^-$) angle of 7-32° (for Nα or Nβ proximal hydroxide groups), while the others point upward with angle range of 71-91° (for Eα or Eβ proximal hydroxide groups). The different chemical properties of a nucleophilic or an electrophilic arrangement suggest that the orientation of the s-HO$^-$ groups can be detected experimentally by high-resolution transmission electron or atomic-force microscopy. A limitation of this minimalist model is that the distal s-HO$^-$ groups all fold down and point away (164-180°) from the central honeycomb due to the incomplete outer sphere honeycombs.

Dalton Transaction   ARTICLE

Table 4 Summary of the distances (Å) between the bridging oxide anions (b-O²⁻) and their centroid (X_{b-O}), out-of-plane movement of the centroid (η_{Si}, Å), and relative diameter of the Si-honeycomb (d_{Si}(experimental) = 5.69 Å) as function of levels of theory in crystalline phase and exfoliated state of kaolinite.

Level of theory	α_p-b-O²⁻	β_p-b-O²⁻	α_d-b-O²⁻	β_d-b-O²⁻	η_{Si}	Δd_{Si}
		crystalline phase				
experimental[19,20]	2.34	2.35 2.35	2.83	2.81 2.80	0.00	0.00
		periodic crystalline model 1×1×1				
PW91/ECP	2.41	2.42 2.42	2.97	2.91 2.91		0.21
PW91/DZ*	2.38	2.38 2.38	2.88	2.85 2.84		0.08
BP86/DZ*	2.39	2.39 2.39	2.88	2.85 2.84		0.09
PW91/TZ*	2.42	2.41 2.41	2.83	2.80 2.79		0.07
BP86/TZ*	2.44	2.44 2.44	2.82	2.79 2.78		0.08
		exfoliated state without an experimental reference				
		periodic slab model 2×2				
PW91/ECP	2.35	2.36 2.36	3.06	3.00 3.00		0.23
PW91/TZ*	2.29	2.30 2.32	2.92	2.89 2.88		0.04
BP86/TZ*	2.31	2.31 2.31	2.93	2.88 2.89		0.05
		molecular cluster model for the Si-honeycomb				
B3LYP/DZ	2.27	2.27 2.27	2.92	2.86 2.86	-0.08	0.00
HF/TZ*	2.38	2.36 2.36	2.85	2.76 2.76	-0.04	0.05
B3LYP/TZ*	2.35	2.34 2.35	2.84	2.80 2.79	-0.04	0.02
PW91/TZ*	2.32	2.32 2.33	2.84	2.79 2.79	-0.03	0.03

Honeycomb Cluster Model for the T-sheet in the Absence of External Chemical Environment

Modelling was also carried out for the position of the b-O²⁻ anions at the surface of the T-sheet, which were monitored by the centroid $X_{b-O}\cdots$b-O²⁻ distances as summarized in Table 4. Differentiation between the proximal and distal b-O²⁻ positions was made based on short (2.34-2.35 Å) and long (2.80-2.83 Å) centroid $X_{b-O}\cdots$b-O²⁻ distances. There is a small difference between the b-O²⁻ anions adjacent to the i-HO⁻ (α) in comparison to the a-O²⁻ groups (β). To a smaller extent, this was observed for the s-HO⁻ groups, which indicate increased covalent and ionic binding of the Si⁴⁺ ion to the O²⁻ groups than the Al³⁺ ion to the HO⁻ groups. In the periodic model of the crystalline phase, the basis set converges at the TZ* level; however, the agreement worsens relative to the experimental values. This is the same observation as we did for modelling of the O-sheet. With the given set of GGA functionals, it is not possible to obtain a better agreement than 0.06-0.08 Å for the proximal b-O²⁻ anions, while the distal b-O²⁻ anion and Si-honeycomb centroid distances are within 0.02 Å. In the periodic exfoliated model, the proximal b-O²⁻ anions move closer to their centroid by about 0.05 Å relative to the crystal structure, while the distal b-O²⁻ anions move away by nearly twice as much (0.07-0.09 Å). The horizontal rearrangement of the b-O²⁻ anions is another significant structural difference between the periodic crystalline and exfoliated molecular nanoclay.

The molecular cluster models reproduce the periodic slab calculations for the proximal b-O²⁻ anions reasonably well. There is a larger deviation between these two calculations for the distal b-O²⁻ anions. This can be correlated with the limitation of the current honeycomb model that describes completely only the inner coordination sphere of the three proximal groups and their adjacent Si⁴⁺ ions. Furthermore, we observe here a significant (0.04–0.06 Å) difference between the levels of theory. As indicated above for the arrangements of the s-OH⁻ groups, the HF wave function based method no longer gives comparable results to the DFT methods. The sinking of the centroid (X_{b-O}) of the six b-O²⁻ anions away from the centre of the exfoliated OT-layer of the kaolinite is also notable (0.03–0.04 Å).

The diameter of the Si-honeycomb closely matches that of the Al-honeycomb in the crystalline structure. The high similarity between the Si- and Al-honeycomb dimensions gives an overall isostructural O- and the T-sheets, which contributes to the formation of the flat OT-sheets that can stack and form the crystalline phase. However, upon exfoliation any expansion (mainly for the T-sheet) and shrinkages (for the O-sheet) relative to the optimized crystal structure will results in surface curvature. This suggests that the nanoclay materials are not expected to be flat, but form bowl shaped platelets. Indeed, experimentally it can be observed that well crystallized exfoliated clay sheets can form scrolls and tubes.[17]

Explicit Aqueous Solvation of Surface Hydroxide Groups

In order to evaluate the reactivity difference of s-HO⁻ groups in electrophilic/nucleophilic or Lewis acid/base orientation, we carried out a additional studies by considering a ring of 6 H₂O molecules as explicit solvent environment on top of the honeycomb model of the O- and T-sheets. The two orientations of the six s-HO⁻ groups define 64 structures with complementary H-bond donor (D) or H-acceptor (A) interactions for the electrophilic (E) and nucleophilic (N) arrangements. Thus, the centroid $X_{s-OH}\cdots$O-H(s-OH⁻) angle between 60°-120° will be considered as H-bond donors (E), and those between 0°–60° (folded in) or 120°–180° (folded out) are H-bond acceptors (N).

The initial 64 structures with 6 water molecules were generated by setting the donor and acceptor s-HO⁻ groups to have $X_{s-OH}\cdots$O-H(s-OH⁻) angle of 66°(α_p), 72°(β_p), 115°(α_d), 107°(β_d) and 10°(α_p), 10°(β_p), 179°(α_d), 171°(β_d), respectively. The O(s-OH⁻)$\cdots$H-OH and H(s-OH⁻)$\cdots$OH₂ distances were set equally to 2.0 Å. When the initial H₂O$\cdots$HOH distances are set to about 1.82±0.06 Å, the size of the ring of 6 H₂O molecules matches the size of the Al-honeycomb. A large number of computations were carried out initially at the PM7 semi-empirical level with COSMO polarizable continuum model (CPCM) of the water solvent (ε=78.4). The spread of the single point energies relative to the lowest energy structure is shown in the left hand side of Fig. 5A. The initial arrangements of the s-HO⁻ groups and the solvent water molecules clearly favours the formation of a strong H-bonding interaction with all s-OH⁻ groups being folded in (A-A-A-A-A-A) and disfavours the crystallographic arrangement (D-D-D-D-D-D), where the order of the s-OH⁻ groups matches those listed in Tables 1 and 2. When the 'x' and 'y' coordinates of the inner sphere atoms of the Al-honeycomb model were allowed to relax with 'z' directional movements restricted (PM7 CPCM z-coordinates fixed results in Fig. 5A), the spread of the relative energies increase. The crystallographic orientation remains the highest energy for the exfoliated state, while structures with folded α-s-HO⁻ orientation or H-bond acceptor positions and β-s-OH⁻ in perpendicular or H-bond donor positions become the lowest
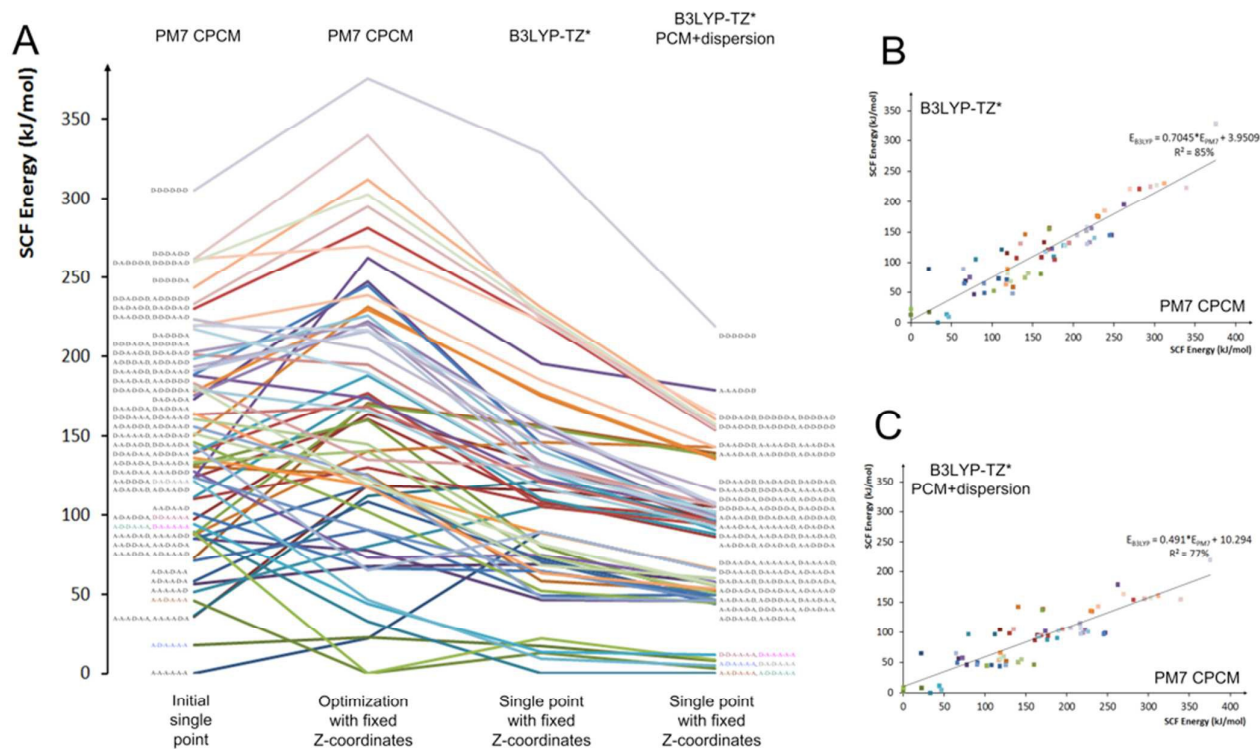
Fig. 5 Summary of calculations for the orientation of *s*-HO⁻ groups in the molecular cluster model of the Al-honeycomb (A) with initial structures, optimized z-coordinates at PM7+CPCM level (left hand side) and single point calculations at the hybrid DFT level with PCM and dispersion correction on the optimized structure with frozen z-coordinates (right hand side). Colour coding in panel A corresponds to structures in Fig. 6. Panels B and C show the correlation of SCF energies from approximate PM7, B3LYP/TZ* and B3LYP/TZ*+PCM levels of theory.

energy structures (green lines at the bottom of Fig. 5, A-A-D-A-A-A and A-D-D-A-A-A). It was remarkable to observe that by increasing the level of theory to B3LYP/TZ*, single point calculations on the PM7+CPCM optimized structures with frozen z-coordinates showed clustering of the energy levels. The final structures of this large-scale computational mapping of relative energies were obtained using the B3LYP hybrid DFT method supplemented with polarization continuum model for water solvent and dispersion correction (right hand side of Fig. 5A). The calculations at the most complete theoretical level with partial optimizations of the inner sphere environment indicate that there will be only 6 different structures out of the total of 64 that we need to consider in further studies for the orientation of the surface hydroxide groups in aqueous environment.

The negligible computational cost of the semi-empirical PM7+CPCM level in comparison to the hybrid DFT with saturated TZ* basis set calculations is attractive. Therefore, we correlated the relative energies of these methods as shown in Figs. 5B and 5C. The correlation is only of 77% and 85% (R^2 values) and the absolute values deviate by 30% due to underestimating the relative energy differences at the semi-empirical level. The dispersion corrected absolute values deviated by more than 50% due to the lack of dispersion correction in the PM7+CPCM calculations for the Al and Si centres. However, we consider that the 77-85% correlation is

already reasonable for using PM7+CPCM method as an initial survey of a large set of structures or providing a low-level quantum chemical method in integrated QM/QM or QM/QM/MM calculations.[49]

Starting from 7 initial structures as summarized Fig. 6, we carried out full structural optimizations for the inner sphere atoms of the molecular cluster model for the Al-honeycomb and the ring of 6 water molecules. The gas phase B3LYP/TZ* calculations in the presence of the explicit water solvent molecules resulted in 7 stationary structures, but with considerable energetic rearrangements relative to the initial PM7+CPCM structures (left hand side of Fig. 6). In the light of the *in vacuo* results from above, it is expected that the lowest energy structures correspond to where the *s*-HO⁻ above the *i*-HO⁻ group (α) is folded in for acceptor position (Aα) with various combinations for the β-*s*-HO⁻ groups. The experimentally observed arrangements of *s*-HO⁻ groups (Dα-Dβ-Dβ) as in the crystalline kaolinite was not found to be the stationary structure at any of the levels of theory either in gas or solution phase models. While the simulations without external chemical environment (Fig. 4 and Table 2) only showed practically two energetically accessible orientations; the external chemical environment defined by explicit solvent water molecules gives 7 well-defined stationary structures.

The inclusion of implicit solvation model and dispersion correction in addition to explicit solvent environment alters
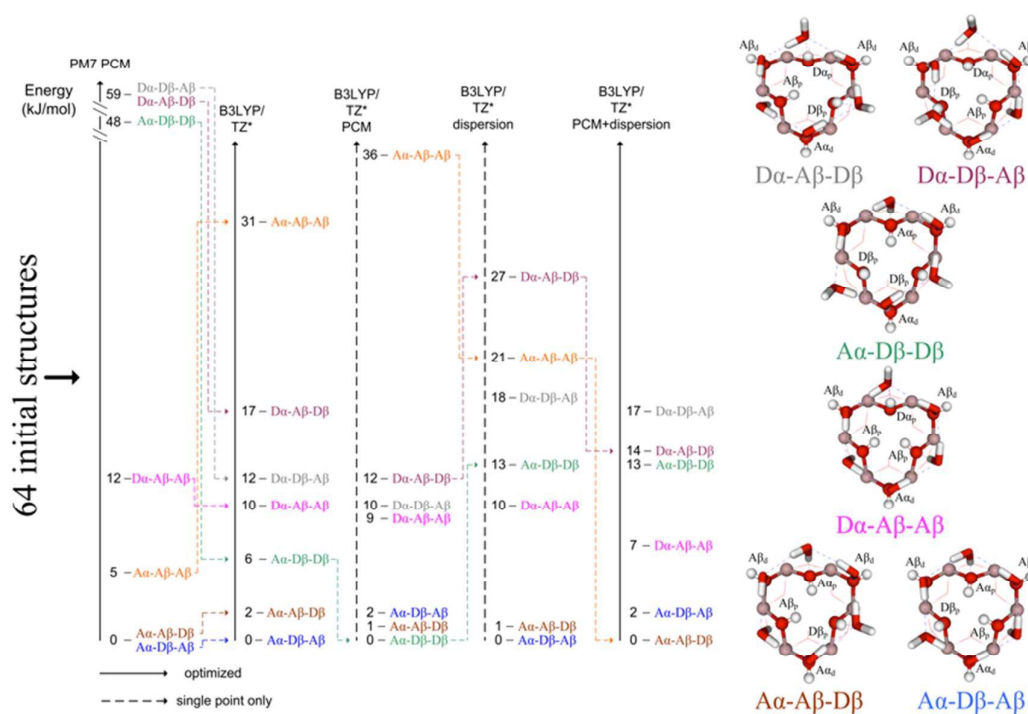
Fig. 6. The potential energy landscape for the orientations for the s-OH$^-$ groups in the presence of six explicit solvent H$_2$O molecules in the molecular cluster model of the Al-honeycomb of exfoliated kaolinite.

the relative energies. They even change the energy ordering from single point energy calculations (see energy levels corresponding to the vertical axis with dashed lines in the middle of Fig. 6). Therefore, we carried out further optimizations with the most comprehensive level of theory (B3LYP/TZ*+PCM+dispersion correction), which resulted in 4 groups of different energy levels and 6 stationary structures. The lowest two orientations (Aα-Aβ-Dβ and Aα-Dβ-Aβ) can be considered as enantiomers due to an approximate mirror image relationship (see bottom right hand side of Fig. 6). The 2 kJ mol^{-1} energy difference is due to the slightly different arrangements of the water molecules on top of the surface. These two structures are well separated by 7 kJ mol^{-1} from the Dα-Aβ-Aβ, which was found to be the highest energy structure for the clean surface models (Fig. 4). The effect of external chemical environment in determining the surface structure is well exemplified by the Aα-Dβ-Dβ orientation, which is among the second highest group of structures, while this was practically degenerate in the *in vacuo* models with the lowest energy structures. This is the result of the relative differences in the strength of ion/dipole interaction between the s-HO$^-$ groups and the H-bonding interactions between the s-HO$^-$ group and explicit solvent H$_2$O molecules. The (H$_2$O)$_6$ cluster sits on top of the surface at a shorter 1.66–1.72 Å and longer 1.89–2.55 Å distances for acceptor O(s-OH$^-$)¨H-OH and donor H(s-OH$^-$)¨OH$_2$ interactions, respectively (Table 5). The initial H$_2$O¨HOH distances of ~1.82(12) Å change to 1.89(10) Å at B3LYP/TZ*+PCM+D level upon optimization. This corresponds to a slightly activated H-bond interaction due to the presence of the kaolinite surface, since the ring of six water molecules

calculated at the same level of theory without the kaolinite surface shows H$_2$O¨HOH distances of 1.71 Å.

As the distal s-HO$^-$ groups fold out of the Al-honeycomb (X$_{s\text{-HO}}$¨O-H(s-HO$^-$) angles are about 180°), they uniformly adopt a H-bond acceptor positions and the H¨O distances range 1.65–1.77 Å with an average value of 1.71±0.03. The last two orientations in Table 5 (Dα-Aβ-Dβ and Dα-Dβ-Aβ) have H¨O distances that are longer than 2.5 Å, which are due to one of the absorbed water molecules forming two H-bonds as it lands in the outer solvation shell. However, these structures are at 17 and 13 kJ mol^{-1} above the lowest energy structure and their contribution to the overall structure is negligible. It is also notable that the lowest energy orientations (Aα-Aβ-Dβ and Aα-Dβ-Aβ) have the shortest H¨O distances, which indicate the presence of the strongest H-bonding interactions.

Explicit Aqueous Solvation Model for the Bridging Oxide Anions

A more limited in scope, but similar analysis was carried out for the b-O^{2-} anions at the surface of the T-sheet compared to the s-HO$^-$ groups of the O-sheet. The initial structures were constructed by building a symmetrical ring of six water molecules on the top of the T-sheet model with initial O¨HOH distances of 2 Å. Similarly to the Al-honeycomb, the size of the Si-honeycomb matches the size of (H$_2$O)$_6$ cluster with H$_2$O¨HOH initial distances of ~1.84(11) Å. This optimizes to 1.79(1) Å at B3LYP/TZ*+PCM+D level, which is shorter than the comparable distances at the O-sheet surface model (1.89 Å). The former value is closer to the kaolinite surface free H$_2$O…HOH distances (1.71 Å). This is indicative of considerably weaker b-O^{2-}…HOH interactions. The top section of Table 6

Table 5 Summary of s-HO$^-$ group orientations expressed by the centroid $X_{s\text{-}HO}$···O-H(s-HO$^-$) angle (degrees) and H···O distances (Å) in H-bonding interactions at B3LYP/TZ*+PCM+D levels of theory in the exfoliated molecular cluster model with a ring of six water molecules on top of the Al-honeycomb.

orientation	α_p	β_p	β_p	α_d	β_d	β_d
Aα-Aβ-Dβ	13.7	17.1	100.9	178.1	176.3	177.1
Aα-Dβ-Aβ	14.0	100.1	16.1	177.8	177.1	176.0
Dα-Aβ-Aβ	102.4	15.0	16.3	179.5	177.9	177.7
Aα-Dβ-Dβ	4.5	104.2	99.6	177.0	178.1	178.2
Dα-Aβ-Dβ	91.1	5.7	82.9	178.5	178.6	177.3
Dα-Dβ-Aβ	87.0	88.5	4.8	178.0	177.5	177.7
H-bonding [a]	α_p	β_p	β_p	α_d	β_d	β_d
Aα-Aβ-Dβ	1.69	1.72	1.89	1.72	1.77	1.72
Aα-Dβ-Aβ	1.70	1.89	1.71	1.69	1.75	1.76
Dα-Aβ-Aβ	1.91	1.70	1.72	1.73	1.73	1.76
Aα-Dβ-Dβ	1.67	1.93	1.93	1.65	1.74	1.70
Dα-Aβ-Dβ	1.94	1.66	2.55	1.69	1.72	1.69
Dα-Dβ-Aβ	2.48	1.92	1.69	1.69	1.68	1.72

[a] O(s-OH$^-$)···H-OH and H(s-OH-)…OH2 distances are shown for acceptor (A) and donor (D) interactions

Table 6 Summary of distances (Å) involving b-O^{2-} anions for Si-honeycomb model of exfoliated kaolinite T-sheet between centroid $X_{b\text{-}O}$ and H atoms of the H-bonded water molecules.

Level of theory	α_p		β_p	α_d	β_d	
$X_{b\text{-}O}$···b-O^{2-} (Å)						
B3LYP/TZ*	2.35	2.35	2.36	2.84	2.80	2.80
B3LYP/TZ*+PCM	2.36	2.36	2.36	2.82	2.77	2.77
B3LYP/TZ*+PCM+D	2.35	2.34	2.36	2.83	2.78	2.78
H-bonding						
B3LYP/TZ*	2.87	2.36	2.31	3.11	2.32	2.33
B3LYP/TZ*+PCM	2.09	1.96	1.95	2.20	1.93	1.94
B3LYP/TZ*+PCM+D	2.01	1.89	1.87	2.00	1.83	1.85

shows the positions of the b-O^{2-} anions not being affected as a function of level of theory by more than 0.01–0.02 Å relative to the clean surface model from Table 2. The Si^{4+}-O^{2-}-Si^{4+} interaction appear to be difficult to affect by H-bonding interaction, which is the opposite to the above discussed Al^{3+}-(OH$^-$)-Al^{3+} interaction, where the orientation of the s-HO$^-$ groups can vary greatly as a result of internal and external ion/dipole and H-bonding interactions. The bottom of Table 6 compares the distances between the H-bond donor of the H$_2$O molecule and the b-O^{2-} acceptor ions. The effect of polarizable continuum model and dispersion correction is dramatic. These clearly highlight the need for using both implicit solvation models in addition to explicit solvent environment as well as a correction for dispersion interactions for achieving chemical accuracy.

Furthermore, it is worth emphasizing the role of hydroxide groups in determining the surface properties of exfoliated kaolinite. For the Al-honeycomb model, we saw the different behaviour of s-HO$^-$ groups above the i-HO$^-$ group. For the Si-honeycomb model, we calculated about 0.1 Å difference between the H-bonding interaction for the α- $versus$ the β-s-HO$^-$ groups. This can be rationalized by the earlier observation where the i-HO$^-$ group changes its orientation upon exfoliation and form a strong directional H-bonding interaction with the diagonal b-O^{2-} anion. This reduces the nucleophilicity of this b-O^{2-} anion, which in turn results in a weaker H-bonding interaction as can be also judged from the elongated H-bonding distance of 2.01 $versus$ 1.88 Å with the explicit solvent H$_2$O molecules relative to b-O^{2-} anions in between two a-O^{2-} anions. These results provide a confirmation of self-consistency of previously seen changes in the position and orientation of the i-HO$^-$ group that was obtained for an independent molecular cluster model developed separately.[7]

Conclusions

Our holistic approach to the modelling of the surfaces of exfoliated kaolinite revealed a remarkably complex network of interaction between the OT-sheet and its external chemical environment. The position and orientation of the surface hydroxide groups are ill-defined in in $vacuo$ models. This results in multiple energetically degenerate orientations. However, this is not a random distribution. We localized preferred orientations and evaluated their stability as a function of levels of theory. Overall, the 8 possible orientations for 3 proximal surface hydroxide groups resulted only 2 energy levels with 3 stationary structures excluding potential enantiomers. At temperatures below the dehydroxylation threshold (~350 °C), there will be one dominant surface arrangement for the exfoliated kaolinite OT-sheet. The surface hydroxide above the inner-hydroxide folds in parallel with the O-sheet, while others remain perpendicular as in the crystal structure.

We localized only 7 stationary structures from the total of 64 possibilities for surface hydroxide groups being H-bond donors or acceptors when considering a ring of water molecules. The use of implicit polarizable solvent models and dispersion correction eliminated a stationary structure. Among the remaining 6 structures only one enantiomer pair will be energetically relevant with a folded surface hydroxide above the inner hydroxide group. In addition, an additional hydroxide group may also point toward the centre of the Al-honeycomb.

With respect to computational methodology, the HF method no longer gave comparable results to DFT methods, which is an opposite conclusion to the inner surface hydroxide study. We also urge using at least triple-ζ basis set with polarization functions for achieving basis set saturation. We found a correlation between the energies calculated by the low-cost PM7+COSMO method and those of hybrid DFT calculations with large basis set, polarizable continuum model, and dispersion correction. This suggest that the semi-empirical Hamiltonian can be effective in screening a large set of structures and providing pre-optimizations a $priori$ to higher level and considerably more expensive DFT calculations.

The self-consistence between our previous study on the inner-hydroxide environment and the compositionally and structurally ill-defined surface hydroxide position and orientation is also notable. These studies used different molecular cluster models, focused on different chemical phenomena and structural features, yet they came to identical conclusions with respect to large-scale structural reorganization in going from crystalline to exfoliated state.

We conclude that the molecular cluster model is a viable approach to modelling surface phenomena for exfoliated

kaolinite. We critically evaluated our cluster models and pointed out a limitation in capturing the full network of weak interactions. As a fix, an algorithm is being developed for generating neutral, counter-ion free nanoparticle models by replacing the sphere of neutralizing ions with protons. These models are expected to allow for constraint free potential energy surface calculations for deeper insights into the tantalizing kaolinite reactivity.

Acknowledgements

Notes and references

‡ **Keywords**: exfoliated kaolinite, surface hydroxide groups, bridging oxide anions, OT-layer, density functional theory, semi-empirical Hamiltonians, molecular cluster modelling

1   A. Lerf, *Dalton Trans.*, 2014, **43**, 10276-10291.
2   H. Cheng, Q. Liu, J. Yang, S. Ma and R. L. Frost, *Thermochim. Acta*, 2012, **545**, 1-13.
3   E. Horvath, J. Kristof and R. L. Frost, *Appl. Spectrosc. Rev.*, 2010, **45**, 130-147.
4   X.-P. Li, H. Yang, Z.-F. Tian, J.-L. Liu and X.-M. Ren, *Dalton Trans.*, 2015, **44**, 4665-4670.
5   Q. Qiao, H. Yang, J.-L. Liu, S.-P. Zhao and X.-M. Ren, *Dalton Trans.*, 2014, **43**, 5427-5434.
6   A. Táborosi, R. Kurdi and R. K. Szilagyi, *Hung. J. Ind. Chem.*, 2014, **42**, 19-23.
7   A. Táborosi, R. Kurdi and R. K. Szilágyi, *Phys. Chem. Chem. Phys*, 2014, **16**, 25830-25839.
8   A. Táborosi and R. K. Szilagyi, *Clay and Clay Min.*, 2015, **50**, CM2015_2001_Taborosi - in press.
9   R. Solc, M. H. Gerzabek, H. Lischka and D. Tunega, *Geoderma*, 2011, **169**, 47-54.
10   H. Man-Chao and Z. Jian, *Chinese Phys. Lett.*, 2012, **29**, 036801.
11   C. Zhang, Y. H. Qi, P. Qian, M. J. Zhong, L. Wang and H. Z. Yin, *Comp. Theo. Chem.*, 2014, **1046**, 10-19.
12   L. Benco, D. Tunega, J. Hafner and H. Lischka, *J. Phys. Chem. B*, 2001, **105**, 10812-10817.
13   L. Benco, D. Tunega, J. Hafner and H. Lischka, *Am. Mineralogist*, 2001, **86**, 1057-1065.
14   R. T. Cygan, J. J. Liang and A. G. Kalinichev, *J. Phys. Chem. B*, 2004, **108**, 1255-1266.
15   J. Shang, M. Flury, J. B. Harsh and R. L. Zollars, *Colloids Surf. A-Physicochem. Engng. Aspects*, 2010, **353**, 1-9.
16   X. L. Hu and A. Michaelides, *Surf. Sci.*, 2008, **602**, 960-974.
17   B. Zsirka, E. Horvath, E. Mako, R. Kurdi and J. Kristof, *Clay and Clay Min.*, 2015, **2015**, CM2015_2017_Zsirka - in press.
18   V. Vagvolgyi, J. Kovacs, E. Horvath, J. Kristof and E. Mako, *J. Colloid Interface Sci.*, 2008, **317**, 523-529.
19   L. Smrcok, D. Tunega, A. J. Ramirez-Cuesta and E. Scholtzova, *Phys. Chem. Minerals*, 2010, **37**, 571-579.
20   R. B. Neder, M. Burghammer, T. Grasl, H. Schulz, A. Bram and S. Fiedler, *Clays and Clay Minerals*, 1999, **47**, 487-494.
21   A. Belsky, M. Hellenbrandt, V. L. Karen and P. Luksch, *Acta Crystallog. B - Struct. Sci.*, 2002, **58**, 364-369.
22   G. Bergerhoff, R. Hundt, R. Sievers and I. D. Brown, *J. Chem. Inf. Comput. Sci.*, 1983, **23**, 66-69.
23   K. N. Kudin and G. E. Scuseria, *Chem. Phys. Lett.*, 1998, **289**, 611-616.
24   K. N. Kudin and G. E. Scuseria, *Phys. Rev. B*, 2000, **61**, 16440-16453.
25   K. N. Kudin, G. E. Scuseria and H. B. Schlegel, *J. Chem. Phys.*, 2001, **114**, 2919-2923.
26   M. J. T. Frisch, G. W.; Schlegel, H. B.; Scuseria, G. E.; Robb, M. A.; Cheeseman, J. R.; Scalmani, G.; Barone, V.; Mennucci, B.; Petersson, G. A.; Nakatsuji, H.; Caricato, M.; Li, X.; Hratchian, H. P.; Izmaylov, A. F.; Bloino, J.; Zheng, G.; Sonnenberg, J. L.; Hada, M.; Ehara, M.; Toyota, K.; Fukuda, R.; Hasegawa, J.; Ishida, M.; Nakajima, T.; Honda, Y.; Kitao, O.; Nakai, H.; Vreven, T.; Montgomery, J. A., Jr.; Peralta, J. E.; Ogliaro, F.; Bearpark, M.; Heyd, J. J.; Brothers, E.; Kudin, K. N.; Staroverov, V. N.; Kobayashi, R.; Normand, J.; Raghavachari, K.; Rendell, A.; Burant, J. C.; Iyengar, S. S.; Tomasi, J.; Cossi, M.; Rega, N.; Millam, N. J.; Klene, M.; Knox, J. E.; Cross, J. B.; Bakken, V.; Adamo, C.; Jaramillo, J.; Gomperts, R.; Stratmann, R. E.; Yazyev, O.; Austin, A. J.; Cammi, R.; Pomelli, C.; Ochterski, J. W.; Martin, R. L.; Morokuma, K.; Zakrzewski, V. G.; Voth, G. A.; Salvador, P.; Dannenberg, J. J.; Dapprich, S.; Daniels, A. D.; Farkas, Ö.; Foresman, J. B.; Ortiz, J. V.; Cioslowski, J.; Fox, D. J., *Gaussian 09*, (2009) Gaussian, Inc., Wallingford CT.
27   B. Miehlich, A. Savin, H. Stoll and H. Preuss, *Chem. Phys. Lett.*, 1989, **157**, 200-206.
28   C. T. Lee, W. T. Yang and R. G. Parr, *Phys. Rev. B*, 1988, **37**, 785-789.
29   A. D. Becke, *Phys. Rev. A*, 1988, **38**, 3098-3100.
30   J. P. Perdew and Y. Wang, *Phys. Rev. B*, 1992, **45**, 13244-13249.
31   J. P. Perdew, J. A. Chevary, S. H. Vosko, K. A. Jackson, M. R. Pederson, D. J. Singh and C. Fiolhais, *Phys. Rev. B*, 1992, **46**, 6671-6687.
32   A. D. Becke, *J. Chem. Phys.*, 1993, **98**, 5648-5652.
33   J. C. Slater, *Phys. Rev.*, 1951, **81**, 385-390.
34   P. Fuentealba, H. Stoll, L. Vonszentpaly, P. Schwerdtfeger and H. Preuss, *J. Phys. B-At. Mol. Opt. Phys.*, 1983, **16**, L323-L328.
35   P. Fuentealba, H. Preuss, H. Stoll and L. Vonszentpaly, *Chem. Phys. Lett.*, 1982, **89**, 418-422.
36   R. Ditchfield, W. J. Hehre and J. A. Pople, *J. Chem. Phys.*, 1971, **54**, 724-728.
37   W. J. Hehre, R. Ditchfield and J. A. Pople, *J. Chem. Phys.*, 1972, **56**, 2257-2261.
38   A. Schäfer, H. Horn and R. Ahlrichs, *J. Chem. Phys.*, 1992, **97**, 2571-2577.
39   A. Schäfer, C. Huber and R. Ahlrichs, *J. Chem. Phys.*, 1994, **100**, 5829-5835.
40   K. L. Schuchardt, B. T. Didier, T. Elsethagen, L. S. Sun, V. Gurumoorthi, J. Chase, J. Li and T. L. Windus, *J. Chem Inf. Model.*, 2007, **47**, 1045-1052.
41   A. Hollwarth, M. Bohme, S. Dapprich, A. W. Ehlers, A. Gobbi, V. Jonas, K. F. Kohler, R. Stegmann, A. Veldkamp and G. Frenking, *Chem. Phys. Lett.*, 1994, **224**, 603-603.
42   A. Hollwarth, M. Bohme, S. Dapprich, A. W. Ehlers, A. Gobbi, V. Jonas, K. F. Kohler, R. Stegmann, A. Veldkamp and G. Frenking, *Chem. Phys. Lett.*, 1993, **208**, 237-240.
43   T. Clark, J. Chandrasekhar, G. W. Spitznagel and P. V. Schleyer, *J. Comp. Chem.*, 1983, **4**, 294-301.
44   J. Tomasi, R. Cammi, B. Mennucci, C. Cappelli and S. Corni, *Phys. Chem. Chem. Phys.*, 2002, **4**, 5697-5712.
45   A. Klamt and G. Schuurmann, *J. Chem. Soc.-Perkin Trans. 2*, 1993, 799-805.
46   S. Grimme, *J. Comp. Chem.*, 2006, **27**, 1787-1799.
47   D. Tunega, T. Bucko and A. Zaoui, *J. Chem. Phys.*, 2012, **137**, Art.No.: 114105.
48   P. F. Weck, E. Kim and C. F. Jove-Colon, *Dalton Trans.*, 2015, **44**, 12550-12560.
49   L. W. Chung, W. M. C. Sameera, R. Ramozzi, A. J. Page, M. Hatanaka, G. P. Petrova, T. V. Harris, X. Li, Z. F. Ke, F. Y. Liu, H. B. Li, L. N. Ding and K. Morokuma, *Chem. Rev.*, 2015, **115**, 5678-5796.

New insights: Surface hydroxide groups of the O-sheet and bridging oxide anions of the T-sheet adopt very different orientations in the exfoliated kaolinite than in the crystalline phase as a function of the presence and absence external chemical environment that significantly influences clay reactivity.

solvated molecular cluster models for exfoliated kaolinite

O-sheet

T-sheet